# Enhanced Regional Earthquake Catalog With Alaska Amphibious Community Seismic Experiment

Natalia A. Ruppert<sup>1C</sup>, Grace Barcheck<sup>2</sup>, and Geoffrey A. Abers<sup>2P</sup>

1 – University of Alaska Fairbanks, Geophysical Institute, 2156 Koyukuk Drive,

Fairbanks, Alaska 99775; naruppert@alaska.edu; 907-474-7472

2 – Cornell University, Department of Earth and Atmospheric Sciences, 2160 Snee Hall, Ithaca, NY 14853

C - Corresponding author

Data

P - The authors acknowledge there are no conflicts of interest recorded.

#### **Abstract**

The Alaska Amphibious Community Seismic Experiment (AACSE) comprised 75 ocean bottom seismometers and 30 land stations and covered about 650 km along the segment of the subduction zone that includes Kodiak Island, the Alaska Peninsula and the Shumagin Islands between May 2018 and September 2019. This unprecedented onshore/offshore dataset provided an opportunity to compile a greatly enhanced earthquake catalog for the region by both increasing the number of detected earthquakes and improving the accuracy of their source parameters. We use all available regional and AACSE campaign seismic data to compile an earthquake catalog for the region between Kodiak and the Shumagin Islands including the Alaska Peninsula (51°N-59°N, 148°N-163°W). We apply the same processing and reporting standards to additional picks and events as the Alaska Earthquake Center currently uses for compilation of the authoritative regional earthquake catalog. Over 7,200 events (both newly detected and previously reported) have been processed with AACSE data. We added about 30% more events, 60% more phase picks, lowered the magnitude of completeness by about 0.2 on average across the region, and improved location errors. All data has been published in public data archives. In addition, we test the machine-learning earthquake detection and picking algorithm EarthquakeTransformer (EQT) on the AACSE seismic dataset, comparing EQT-determined P and S picks with the new catalog. EQT is entirely trained on land data, while AACSE is amphibious. Overall, EQT finds 59% of P and 63% of S arrivals in the catalog within 300 km epicentral distance. The percent of catalog picks detected by EQT varies inversely with earthquake epicentral distance, and EQT performs particularly poorly on data from earthquakes recorded by instruments in the outer rise.

#### Introduction

The Alaska-Aleutian subduction zone is one of the most active subduction regions in the world. The region has an extensive history of major megathrust earthquakes, including most recently the magnitude 7.6 2020 Simeonof Earthquake in the Shumagin Islands and the magnitude 8.2 2021 Chignik Earthquake southwest of Kodiak Island. The authoritative earthquake catalog for Alaska is produced by the Alaska Earthquake Center (AEC) and utilizes all available real-time regional seismic data for earthquake detections. However, the stations used for these detections are land-based, and therefore earthquake locations and especially depths in the offshore regions are characterized by large uncertainties. The Alaska Amphibious Community Seismic Experiment (AACSE) comprised 75 ocean bottom seismometers (OBSs) and 30 land stations and covered about 650 km along the segment of the subduction zone that includes Kodiak Island, the Alaska Peninsula and the Shumagin Islands between May 2018 and September 2019 (Barcheck et al., 2020). Offshore, OBSs extend from the outer rise to the shallow shelf. This unprecedented amphibious dataset provided an opportunity to produce a greatly enhanced earthquake catalog for the AACSE study area by both increasing the number of detected earthquakes and improving the accuracy of their source parameters.

The AACSE catalog project began in earnest in January 2020. As we now know, the COVID-19 pandemic was beginning to spread across the world at the same time. The premise of the project was to train student analysts to process the data. However, with universities switching to remote learning, student hiring and training became problematic. We had to innovate and restructure our analyst training procedures to adapt to remote video conferencing and working on remote desktops. In the end, the catalog processing took longer than originally anticipated, but after a few delays we were able to bring it to a successful completion.

The enhanced earthquake catalog is based on seismic data recorded by the permanent regional and volcano networks, temporary USArray stations and AACSE OBS and land-based

seismic stations. We follow the same processing standards and guidelines as those being utilized by the Earthquake Center to report and catalog regional earthquakes. We take full advantage of the existing regional seismic catalog and build on it with the addition of automatic and analyst-reviewed seismic phases.

In addition to detecting earthquakes with the standard network methods, we test the performance of the machine-learning earthquake detection and picking algorithm EQTransformer (Mousavi et al., 2020) against the analyst-checked AACSE catalog. A number of powerful machine-learning seismic algorithms have been developed in recent years to automate tasks involved in earthquake catalog creation, such as earthquake detection, phase picking, and phase association (e.g., Ross et al., 2018; Mousavi et al., 2019b; Ross et al., 2019; Zhu et al., 2019; Mousavi et al., 2020; Soto and Schurr, 2021; Zhu et al., 2022). Training complex deep-learning models requires large labeled datasets, which are readily created from existing earthquake catalogs. However, trained deep-learning models do not necessarily transfer well to novel seismic datasets from differing tectonic regimes, noise environments, or network arrangements (e.g., Munchmeyer et al., 2022). The AACSE network is amphibious, with both land and ocean-bottom seismometers, presenting a challenge for earthquake detection using deep-learning models that have, to date, only been trained on land data. We apply EQTransformer to evaluate how well this deep-learning model transfers to the amphibious AACSE seismic dataset, and we document its initial performance in this challenging environment.

## AACSE catalog processing workflow

AEC has been successfully using the Antelope system from Boulder Real Time Technologies (BRTT Inc.) for seismic data acquisition, processing and archival for over 20 years and has developed a set of standard practices for automatic event detections and analyst review.

We applied the same standards for AACSE earthquake catalog processing within the AACSE study area (51°N-59°N, 148°W-163°W).

First, we acquired station metadata for all AACSE sites and corresponding waveforms for seismic sensors and ocean-bottom pressure gauges from the IRIS Data Management Center. Next, the data were merged into the center's in-house waveform archive and station database. Merging of the station metadata and waveforms allowed us to process all available data regardless of the original source.

We then identified the best set of parameters for running STA/LTA (short-term and long-term average) seismic phase detection routines. We tested several options for filters, signal-to-noise ratios, and detection window lengths. We settled on 3 different sets of parameters for ocean bottom broadbands, land-based broadbands, and deep pressure gauges (Table S1).

Next, we designed and tested travel time grids to be used for association of detected arrivals into potential hypocenters. After a number of tests, we decided to use 2 grids: crustal and intermediate depth (Figure S1). The crustal grid covered the entire study region from 0-50 km depth at 5 km intervals; the intermediate depth grid extended along the subduction zone strike between 60-260 km depth at 10 km intervals down to 100 km depth and 20 km intervals deeper. Both grids had horizontal node spacing of about 10 km. We set a minimum of 4 phase detections from 4 different stations required to declare a successful event association.

Lastly, we identified stations with bad data quality or timing issues and removed them from our auto-detection lists. Noisy sites tend to produce too many false detections resulting in bogus events that increase workload on analysts. Moreover, after evaluating automatic detection on pressure gauge channels we decided not to use them for auto-detections. These channels tended to produce too many false triggers.

Earthquake data processing followed these steps:

- Run STA/LTA detector (dbdetect) to detect candidate phases at all stations in the AACSE study area (AACSE plus permanent) with good quality broadband seismic channels for each UTC day; dbdetect is run in a different frequency band for ocean bottom vs land stations.
- 2. Run event associator (*dbgrassoc*) on identified phase detections, associating detections first with preexisting events from AEC catalog and then identifying new events.
- 3. Student analysts manually review all events, new and pre-existing, using the *dbloc2* and *dbpick* programs. Automatic picks are reviewed and adjusted if necessary, and events are relocated using *genloc* and regional velocity models (described below). AEC's standard phase distance weighting was applied (Table S2).
- Supervising seismologist verifies student processing and computes local magnitudes for all events using in-house, custom aeic\_dbml program.

Automatically identified event sources fell into the following categories:

- 1. Pre-existing events within the AACSE region These events were previously reviewed by an AEC analyst without AACSE data, and processing AACSE stations resulted in new auto-detected phase picks. Student analysts reviewed and adjusted all new auto-picks, added missing P and S arrivals, and removed bad arrivals for each event. They then computed the new location (origin), deleted all pre-existing origins and saved the best reviewed origin.
- 2. New events within the AACSE region Usually these would be smaller events that could not be detected with the permanent land-based network stations. Here again we added or corrected all good, clear P and S arrivals and removed bad auto-picks. We then computed the new location, deleted all pre-existing origins and saved our best reviewed origin.
- 3. Other Alaskan events outside of the AACSE region We did not process other Alaskan events outside of the study region. The automatic locations for such out-of-region events tended to be near the edges of the travel time grids. These events were deleted. We chose to keep some events that after relocation fell slightly outside of the study region.

- 4. Teleseismic events (coming from outside of Alaska) These events had clear, usually low-frequency P arrivals, but no detected S arrivals. The depths for such events also tended to be quite deep (>100 km). These events were deleted.
- 5. Bogus events These were formed from various data glitches or noise bursts. These events were deleted.

We used 4 regional plane-layer velocity models for locations: *gulfak* for events in the Gulf of Alaska and outer rise (Table S3), *northak* for shallow crustal events in the overriding plate (Table S4), *pavdut* for events near Shumagin Islands (Table S5), and *scak* for events under Alaska Peninsula and Kodiak Island (Table S6). These models are being used in AEC's catalog processing. A minimum of 6 P-picks was required to process and save an event into the final catalog. With a few exceptions, only events located within the AACSE study area (51°N-59°N, 148°W-163°W) are kept in the final new catalog.

For pre-existing events, we preserved the same magnitudes as were originally reported in the Earthquake Center catalogs, i.e. no AACSE stations were used for recomputing the magnitudes. For new events, local magnitudes were computed using AEC's standard magnitude calculations and all traces with P-phase picks up to 500 km distance. Some stations were influenced by strong structural heterogeneities, especially OBS's near the trench, resulting in amplified amplitudes and elevated magnitude values (Figure S2). All magnitude readings that were more than 1 unit above or below the network mean were excluded for computing the final magnitude value.

The AACSE stations were deployed gradually over the course of about 2.5 months May-July, 2018 and the stations were removed again over the course of about 2 months in August-September, 2019. We processed earthquakes that occurred between May 12, 2018 when the first AACSE stations were installed, through August 31, 2019, about 10 days before the last AACSE station was decommissioned. The mid-May processing start allowed us to get familiar with the network gradually and train student analysts on a dataset with fewer new stations. We chose to

end the catalog processing on August 31, 2019 since only a handful of stations operated beyond that date. These stations would have not provided any new earthquake detections and there would have been very few new picks for the existing events, especially compared with the thousands of new picks already added into the catalog.

After processing, the original CSS Datascope tables were converted into *quakeml* format and uploaded to the USGS's Comcat catalog as AACSE catalog with AK contributor. We also made available monthly Datascope CSS3.0 database tables and *quakeml* files with UA@ScholarWorks publications (Ruppert et al., 2021a-b).

### Processing challenges

As we analyzed the data, we encountered a few challenges. Out of 75 deployed OBS packages, four did not get recovered and three did not record any seismic or hydrophone data. Four additional OBSs did not record any ground motion data on broadband seismometers, while the pressure and hydrophone data were available (Barcheck et al., 2020). Some stations had other data quality issues, such as glitches on some or all components, timing problems, or pegged mass positions, especially further in time into the project. Fortunately, some stations had both broadband and strong motion sensors, and all OBSs had pressure gauges. Our first choice for phase picks at any station was always a broadband sensor, with vertical channels used for P-wave picks and horizontal channels used for S-wave picks. If for any reason arrivals on broadband channels were impossible to discern, we used strong motion (P and/or S arrivals) or pressure (only P arrivals) data channels. As much as possible, we tried to avoid picking on stations with reported timing problems, but we suspect a few picks from such stations still made it into the catalog. Timing problems are documented in Barcheck et al. (2020). For processing, we used the same filters as for auto-detections (Table S1).

Due to very slow seafloor sediments, some OBS stations had small amplitude, emergent arrivals on vertical channels that were not discernable on horizontal channels. As a result, we chose not to pick P arrivals on horizontal channels of OBS stations, while we occasionally used horizontal channels for P picks on land stations. We also occasionally used vertical channels to pick S arrivals on either OBS or land sites.

Another unexpected challenge came from the inability of the *genloc* earthquake location program to use station elevations for OBS sites that were below the top layer of velocity model. For example, the top layer of the *pavdut* model extended to 3 km depth, meaning any OBS site in greater than 3 km water depth was assigned an elevation of 0 km, which may have resulted in higher time residual for phase picks on those stations.

Lastly, strong structural heterogeneities resulted in high RMS residuals for some events, especially those with many OBS stations in the solutions. In particular, large differences exist between continent-like structure beneath arc and forearc, and oceanic lithosphere seaward of the trench (Figure S3). The amplitude of the residuals is highly dependent on the event to station azimuth and distance. We prioritized keeping all picks, even with high travel time residuals, over lowering the overall RMS. At times we had to fix the depth or epicenter location when we could not obtain a reasonable solution with free depth. The resulting dataset then has the potential to be used as a basis for future structural studies.

#### Results and discussion

We analyzed 7,242 earthquakes, 2,279 of which (or 39%) were newly identified events (Figures 1a-b, 2a-b, 3a-b, Table S7). The new catalog contains nearly 440,000 seismic phases total, almost 300,000 of which (or 60%) were new picks (Figure 4). Most of the newly detected earthquakes were in the M7.9 2018 Offshore Kodiak earthquake aftershock region (Ruppert et al., 2018), under Kodiak Island and beneath the Alaska Peninsula (Figure 2b). Overall, distribution

of newly detected events followed long-term seismicity patterns in the region. For example, increase in outer-rise seismicity to the west of 159°W has been observed in regional seismicity maps prior to the project and is most likely caused by real tectonic forcing rather than detection capabilities or processing methods.

Ten largest earthquakes recorded during the project had magnitudes  $M_{WW}$ =4.95 or greater (Table S8). About half of these earthquakes were intraslab events beneath Kodiak Island and Alaska Peninsula with depths ranging between about 50-120 km. The other half were the interface earthquakes that occurred beneath the Shumagin Islands region at depths between about 30-35 km. The largest recorded earthquakes were  $M_W$ =6.0 on December 31, 2018 and  $M_W$ =5.8 on July 19, 2018 in the Shumagin Islands; moment tensor source mechanisms of both events indicate underthrusting on the subduction zone interface. Both events were followed by a couple dozen aftershocks.

Addition of picks from AACSE stations helped to improve hypocentral location quality. Overall mean horizontal and vertical errors improved from 3.81 km and 2.46 km in AEC catalog to 1.83 km and 1.53 km in AACSE catalog, respectively (Figure S4).

Some systematic epicentral shifts are observed for the events located in the outer rise and the Offshore Kodiak aftershock region. Specifically, events in the aftershock cluster shifted southeast by 11.6 km on average (Figure S5).

The magnitude of completeness (M<sub>C</sub>) for the entire region lowered from 2.7 to about 2.5, with varying degrees of success across the region (Table S9, Figure 5). The most significant improvement is observed for the outer rise region, where M<sub>C</sub> decreased from 3.0 to 2.4. Kodiak Island region M<sub>C</sub> lowered from 1.6 to 1.4. Surprisingly, there was no change in M<sub>C</sub> within the Shumagin Islands region. While we were able to detect more events in the upper magnitude 1 - lower magnitude 2 range, Mc value for the enhanced catalog remained at 2.1. This is probably because land-based permanent volcano-monitoring and other regional stations provide

reasonably good detection capabilities. While addition of OBS data contributed to better constrained earthquake locations, they did not necessarily lower the overall detection thresholds.

## Application of EQTransformer to AACSE data

EarthquakeTransformer (EQT) is a deep-learning model capable of detecting earthquakes and phase arrivals, and picking P and S arrival times (Mousavi et al., 2020). The original trained model demonstrates skill by finding roughly 40% more phases and 2.5 times more earthquakes in a region of Japan that was not included in the EQT training dataset, despite using only a third of the stations (Mousavi et al., 2020). The original EQT model was trained on the large STanford EArthquake Dataset (STEAD) containing 1 million earthquakes and 300 thousand noise waveforms (Mousavi et al., 2019a). All STEAD waveforms are recorded by land seismometers within 300 km of earthquakes in a variety of tectonic regimes. However, as we show here, this published EQT model does not necessarily generalize well to the AACSE network, which records earthquakes traveling through complex and diverse subduction zone structures on both land and ocean-bottom instruments.

We test the performance of the original published EQT model (Mousavi et al., 2020) on the AACSE seismic dataset. Because land and ocean-bottom seismometers record in very different noise environments, we use different preprocessing for each instrument type. Default preprocessing for EQT includes a 1-45 Hz bandpass filter, which we apply to the AACSE land data. AACSE ocean-bottom instruments, however, have a much higher noise floor in the ~1-3 Hz band than the AACSE land seismometers (e.g., Barcheck et al., 2020; their Figure 8), and small earthquakes in ocean-bottom data are nearly impossible to see in the 1-45 Hz passband. After testing several filters, we find that using a 5-20 Hz bandpass filter on ocean-bottom data permits EQT to find the highest number of true detections while also eliminating bogus detections on high-

frequency noise sources. We therefore preprocess all ocean-bottom AACSE data using a 5-20 Hz bandpass filter. All other preprocessing is identical to Mousavi et al. (2020).

We apply the EQT earthquake detection and picking model to the filtered continuous AACSE data from 106 stations located between 163°W-148°W and 51°N-60°N (51 land, 55 ocean-bottom) from June 1, 2018 through July 31, 2019, using detection and P/S picking thresholds of 0.3. We processed only good quality data. We then compare EQT P and S picks with phases in AEC's analyst-checked AACSE catalog. We only compare EQT and AEC picks during time periods with good data collected on at least one channel at each of the 106 stations.

Over the 14 months of data processed, the AEC catalog contains roughly 94,000 P and 78,000 S picks within 300 km epicentral distance at the 106 sites processed. Of these, EQT finds 59.0% of P and 63.0% of S arrivals (recall of 0.59 (P) and 0.63 (S)). We do not calculate precisions due to the challenging task of determining the false positive rate for tens of thousands of EQT picks generated from continuous seismic data. Median pick time residuals (AEC AACSE catalog pick time minus EQT predicted pick time) are 0.019 sec (P) and -0.01 sec (S), and the root mean square error is 0.34 sec (P) and 0.38 sec (S) (Figure 6). This rate of arrival recovery is much lower than EQT performance on its test dataset (recall of 0.99 (P) and 0.96 (S)).

EQT picking performance also differs substantially depending on the region of the AACSE network, earthquake epicentral distance, and earthquake depth (Figure 6). EQT is much more successful picking both P and S at AACSE sites closer to an earthquake, regardless of land versus ocean-bottom (Figure 6d-e). Within 100 km, EQT finds 79% of P and 78% of S, while at distances > 250 km, EQT only finds 29% of P and 35% of S. The proportion of arrivals found is similar for land and ocean-bottom instruments, with the notable exception of outer rise sites. There EQT consistently finds fewer P and S arrivals at all distances (purple curves, Figure 6d-e). EQT also appears to be slightly better at finding P arrivals for events with catalog depths of 40-80 km than events at 0-40 km depth or deeper than 80 km (Figure 6j).

Pick time residuals (AEC AACSE catalog pick time minus EQT predicted pick time) show slightly different distributions for land and ocean-bottom instruments. Notably, the median P pick time residual is ~0.05-0.1 seconds for ocean-bottom data but ~0.0 for land data (Figure 6). In other words, EQT P picks on ocean-bottom data are often a fraction of a second early relative to analyst pick times, while land P picks are not. This lag could result from either EQT limitations or analyst error, and it might be problematic for some applications that rely on local earthquake arrival times. In addition, the root mean square error of P pick residuals is slightly larger for ocean-bottom data than land data, suggesting EQT tends to do a poorer job in general picking arrival onset time for ocean-bottom data. Patterns are generally less clear for S arrivals, which are often more difficult for human analysts to pick as well. Histograms of pick residuals broken apart by source-receiver distance, source depth, and network region can be found in Figures S6-S8.

EQT finds far fewer arrivals in the amphibious AACSE dataset than expected, which likely results from limitations in the STEAD training dataset that are relevant for amphibious subduction zone deployments. Foremost, STEAD contains no OBS waveforms, and EQT has therefore never learned to ignore ocean-bottom noise or accommodate waveforms with oceanic paths. For example, water-column multiples and T phases sometimes dominate regional deep-sea waveforms, while Lg is absent. In addition, STEAD has non-subduction-zone paths over-represented: around 60% of the global dataset comes from the lower 48 U.S. states, excluding Cascadia (Mousavi et al., 2019a). EQT may therefore plausibly be less sensitive than expected to earthquakes with subduction zone paths. Also, STEAD contains few subcrustal earthquakes, with only ~8% of waveforms from events deeper than 50 km. The EQT model trained with STEAD encounters challenges when picking arrivals for the variety of earthquakes (e.g., deep, shallow) traversing a mixture of paths (fast cold oceanic crust, slow upper plate, heavily faulted outer rise) and recorded in a variety of noise environments (shallow water, deep water, coastal, inland) in the complex AACSE study area. Nevertheless, the excellent performance of EQT on its test set

suggests that performance in the AACSE region and in subduction zones generally can be improved by transfer learning with more subduction zone and ocean-bottom seismic data.

#### Conclusions

AACSE earthquake catalog covers the region between 148°W-163°W and 51°N-59°N and the time period between May 12, 2018 and August 31, 2019. Enhanced catalog has 40% more events and 60% phase picks as compared to the original catalog produced from the permanent network stations. The magnitude of completeness for the entire region lowered from 2.7 to about 2.5, with varying degrees of success across the region. The 2018 Offshore Kodiak aftershock region and the outer rise showed the most consistent improvements in magnitude of completeness. The largest number of newly detected events fell in the magnitude 2-3 range. More events were detected under the magnitude 2 range as well, but not as many as originally expected. Due to additional station coverage, hypocentral location errors were also reduced.

Strong structural heterogeneities, especially near the trench, resulted at times in higher travel time and magnitude residuals. During processing we prioritized inclusion of all available phase picks over reducing overall RMS error. Future relocation efforts should account for heterogeneous velocity structure.

Testing EQT on the AACSE dataset reveals poor picking performance on the amphibious AACSE data relative to published EQT performance. Of arrivals in the AACSE catalog recorded within 300 km epicentral distance, EQT finds only 59% of P and 63% of S phases. EQT successfully picks more earthquakes at close epicentral distances (<~100 km) for both land and ocean-bottom seismometers, and the rate of successful picking falls off with increasing epicentral distance. With the exception of earthquakes recorded in the outer rise, EQT finds similar proportions of picks in data from land and ocean-bottom seismometers. EQT is particularly bad at picking earthquakes recorded by instruments in the outer rise. In addition, comparing EQT and

AACSE catalog pick times reveals larger median and root-mean-square residuals for P picks on ocean-bottom data in general. We suggest the unexpectedly poor performance of EQT on the amphibious AACSE dataset results from limitations in the STEAD training dataset, for example relatively few subduction zone paths and no ocean-bottom data.

A uniform, publicly available earthquake catalog that leverages both the permanent and temporary stations is now a valuable asset to the research community as well as for regional seismic hazard characterization.

#### Data and resources

Earthquake catalog and phase picks are available from ANSS Comprehensive Earthquake Catalog (Comcat) by selecting catalog "Aacse" from earthquake.usgs.gov/earthquakes/search website. Monthly Datascope CSS3.0 database tables and *quakeml* files are also available for download from UA@ScholarWorks publications (Ruppert et al., 2021a, 2021b). All raw AACSE seismograms are archived in the IRIS Data Center under station code XO 2018-2019 (https://doi.org/10.7914/SN/XO 2018). Supplemental Material includes tables and figures with parametric information and additional information on catalog processing details.

## Acknowledgments

We would like to acknowledge the support of the Alaska Earthquake Center staff and especially student analysts Kenneth Becker and Daneel Ruppert who processed the majority of the earthquakes working from home during the COVID-19 pandemic. We also acknowledge a large number of researchers, the OBSIP and PASSCAL instrument centers and their staffs for making the AACSE project a success, and the IRIS Data Center for data archival. This material is based upon work supported by the U.S. Geological Survey under Grant No. G20AP00026, with data

collected by the AACSE project under National Science Foundation award OCE-1654568 to Cornell. The views and conclusions contained in this document are those of the authors and should not be interpreted as representing the opinions or policies of the U.S. Geological Survey. Mention of trade names or commercial products does not constitute their endorsement by the U.S. Geological Survey.

#### References

- Barcheck, G., G. A. Abers, A. N. Adams, A. Bécel, J. Collins, J. B. Gaherty, P. J. Haeussler, Z. Li, G. Moore, E. Onyango, E. Roland, D. E. Sampson, S. Y. Schwartz, A. F. Sheehan, D. J. Shillington, P. J. Shore, S. Webb, D. A. Wiens, and L. L. Worthington (2020). The Alaska Amphibious seismic Community experiment, *Seims. Res. Lett.* 91 2054-3063, https://doi.org/10.1785/0220200189.
- Mousavi, S.M., Y. Sheng, W. Zhu, and G. C. Beroza (2019a). STanford EArthquake Dataset (STEAD): A Global Data Set of Seismic Signals for AI, *IEEE Access* **7** 179464–179476, doi:10.1109/ACCESS.2019.2947848.
- Mousavi, S.M., W. Zhu, Y. Sheng, and G. C. Beroza (2019b) CRED: A Deep Residual Network of Convolutional and Recurrent Units for Earthquake Signal Detection. *Sci Rep* **9** 10267, https://doi.org/10.1038/s41598-019-45748-1.
- Mousavi, S. M., W. L. Ellsworth, W. Zhu, et al. (2020). Earthquake transformer—an attentive deep-learning model for simultaneous earthquake detection and phase picking. *Nat. Commun.* **11** 3952, <a href="https://doi.org/10.1038/s41467-020-17591-w">https://doi.org/10.1038/s41467-020-17591-w</a>.
- Münchmeyer, J., J. Woollam, A. Rietbrock, F. Tilmann, D. Lange, T. Bornstein, et al. (2022). Which picker fits my data? A quantitative evaluation of deep learning based seismic pickers. *J. Geophys. Res. Solid Earth* **127** e2021JB023499, <a href="https://doi.org/10.1029/2021JB023499">https://doi.org/10.1029/2021JB023499</a>.

- Ross, Z. E., M.-A. Meier, E. Hauksson, and T. H. Heaton (2018). Generalized Seismic Phase Detection with Deep Learning, *Bull. Seism. Soc. Am.* **108** 2894–2901, doi: https://doi.org/10.1785/0120180080.
- Ross, Z. E., Y. Yue, M.-A. Meier, E. Hauksson, and T. H. Heaton (2019). PhaseLink: A deep learning approach to seismic phase association, *J. Geophys. Res. Solid Earth* **124** 856–869, <a href="https://doi.org/10.1029/2018JB016674">https://doi.org/10.1029/2018JB016674</a>.
- Ruppert, N. A., G. Barcheck, and G. Abers (2021a). AACSE earthquake catalog: January-August, 2019, *ScholarWorks@UA*, http://hdl.handle.net/11122/11418.
- Ruppert, N. A., G. Barcheck, and G. Abers (2021b). AACSE earthquake catalog: January-August, 2019, *ScholarWorks@UA*, http://hdl.handle.net/11122/11967.
- Soto, H., and B. Schurr (2021). DeepPhasePick: a method for detecting and picking seismic phases from local earthquakes based on highly optimized convolutional and recurrent deep neural networks, *Geophys. J. Int.* **227** 1268–1294, <a href="https://doi.org/10.1093/gji/gqab266.">https://doi.org/10.1093/gji/gqab266.</a>
- Zhu, W., and G. C. Beroza (2019). PhaseNet: a deep-neural-network-based seismic arrival-time picking method, *Geophys. J. Int.* **216** 261–273, <a href="https://doi.org/10.1093/gji/ggy423.">https://doi.org/10.1093/gji/ggy423.</a>
- Zhu, W., K. S. Tai, S. M. Mousavi, P. Bailis and G. C. Beroza (2022). An end-to-end earthquake detection method for joint phase picking and association using deep learning, *J. Geophys. Res. Solid Earth* **127** e2021JB023283, https://doi.org/10.1029/2021JB023283.

#### Mailing addresses:

- N.A.R.: University of Alaska Fairbanks, Geophysical Institute, 2156 Koyukuk Drive, Fairbanks, Alaska 99775, USA
- G.B. and G.A.A.: Cornell University, Department of Earth and Atmospheric Sciences, 2160 Snee Hall, Ithaca, NY 14853, USA

#### **Figures**

**Figure 1.** Monthly breakdown by new, old and total of (a) analyzed seismic events and (b) picked seismic phases in the AACSE earthquake catalog.

**Figure 2.** Map of (a) all processed events and (b) newly detected events from AACSE earthquake catalog, color-coded by depth. AACSE and permanent seismic stations are shown in (a).

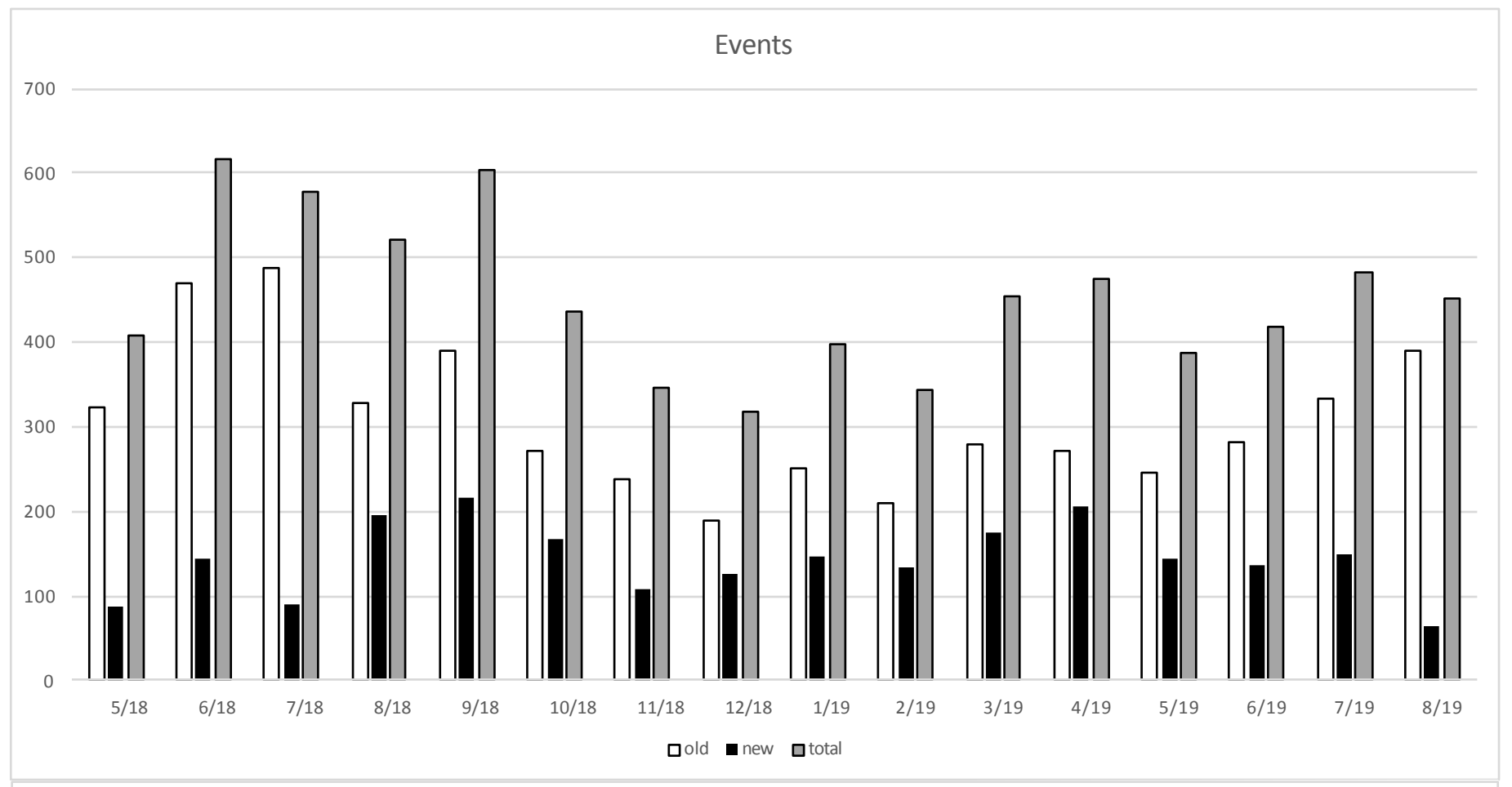
**Figure 3**. Down-dip cross-sections under (a) Kodiak Island and (b) Shumagin Islands. Gray stars indicate earthquakes with magnitudes 5 or greater. Cross-sections include a 150-km wide swath of seismicity.

**Figure 4**. Number of phase picks for events in the AEC catalog for the region (black crosses) superimposed on the number of picks in the AACSE catalog (red circles).

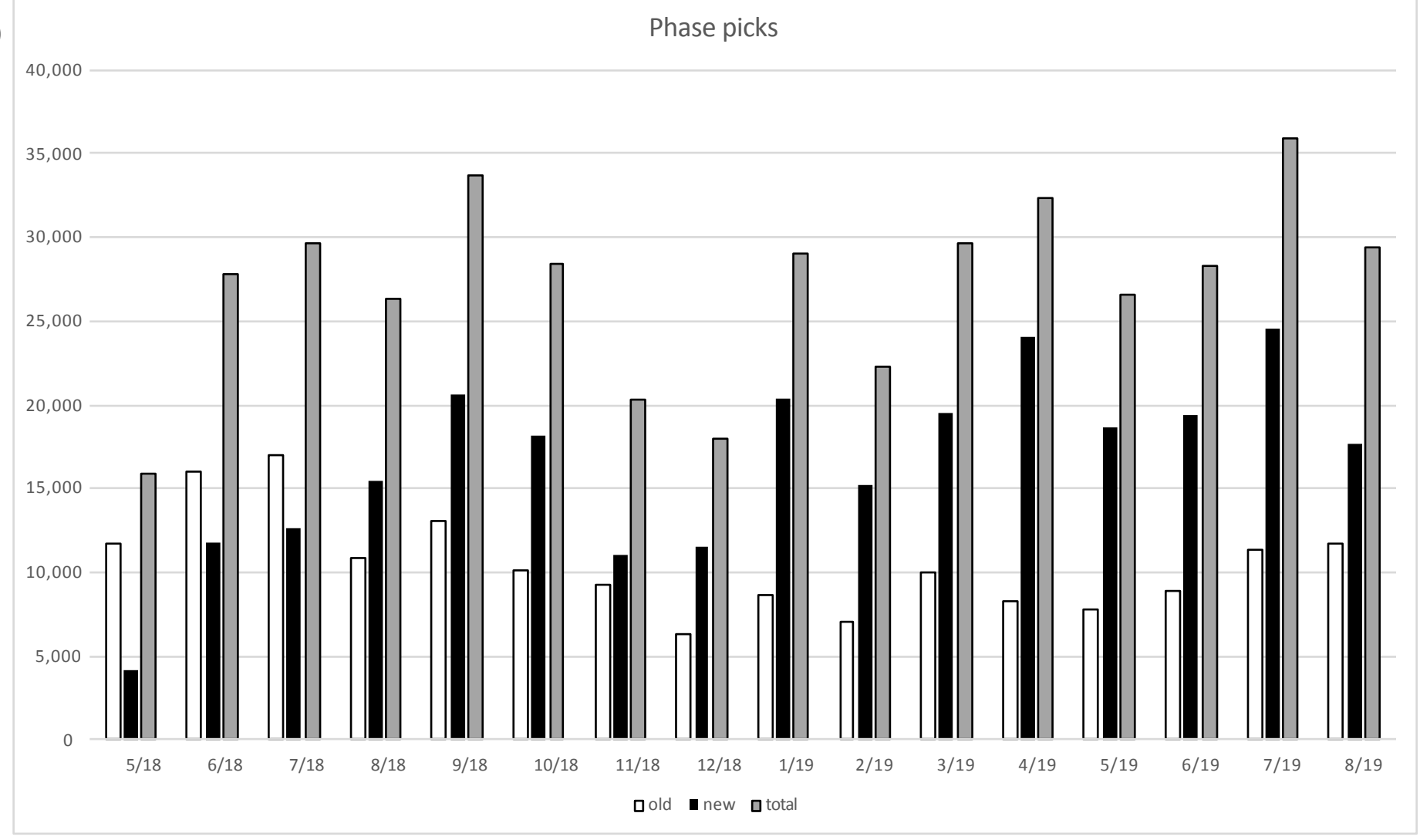
**Figure 5.** Frequency-magnitude distribution of the original AEC earthquake catalog (in red) and enhanced AACSE earthquake catalog (in black).

Figure 6. Results of application of EQTransformer (Mousavi et al., 2020) to the continuous AACSE data. (a) Map of AACSE network, with stations colored by instrument type and network region. (b-c) Histograms of EQTransformer pick residuals (AEC AACSE catalog pick time minus EQTransformer pick time) for P picks (left panel) and S picks (right panel). OUT is the fraction of picks with absolute residuals greater than 0.45 seconds. MAE is mean absolute error. RMSE is root mean squared error. Red and blue vertical lines show the mean and median residual, respectively. Panels (d-i) show residual statistics as a function of network region (colors matching panel (a)) and source-receiver distance. Panels (j-o) show residual statistics as a function of network region (colors matching panel (a)) and earthquake source depth.









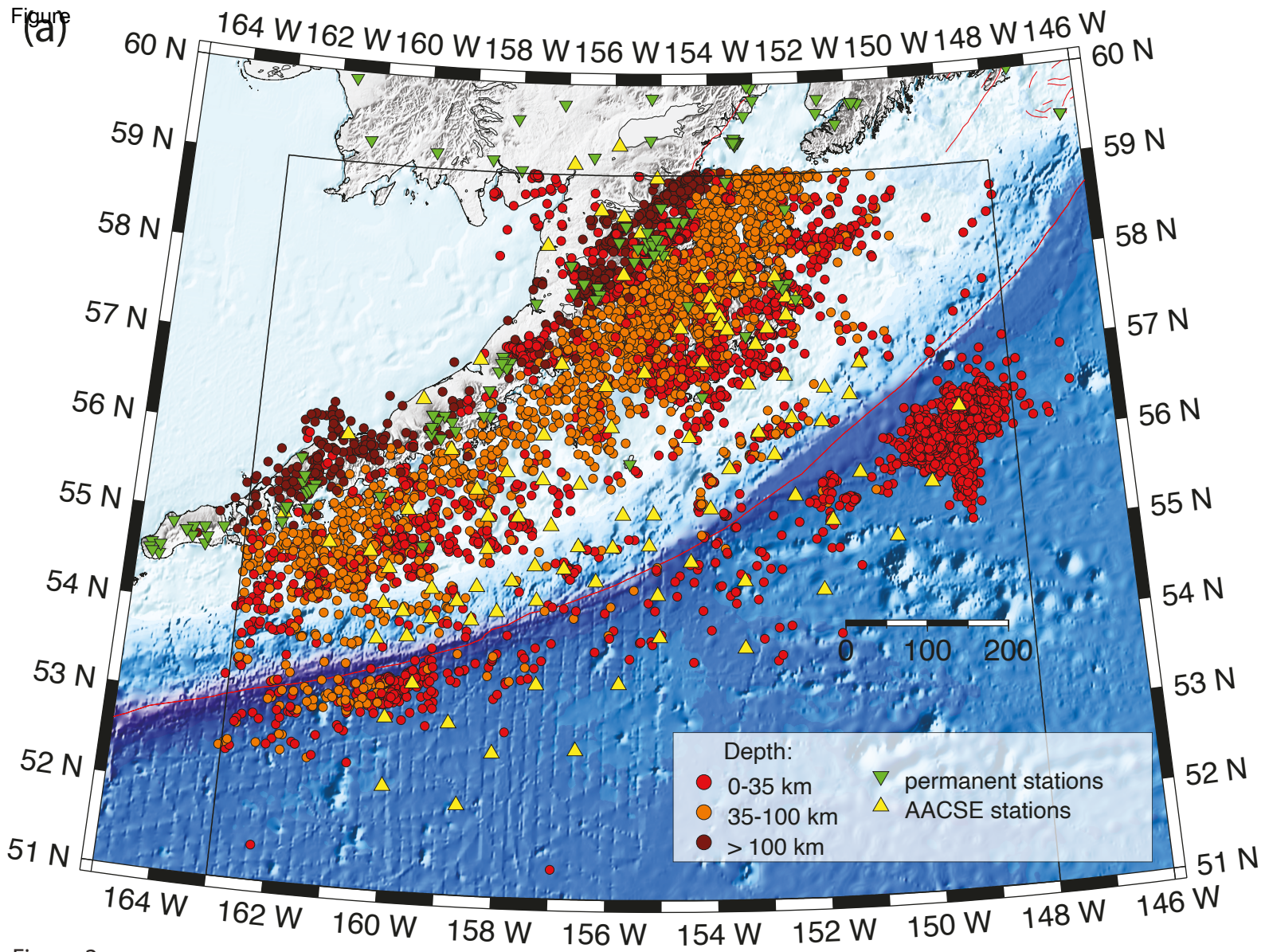
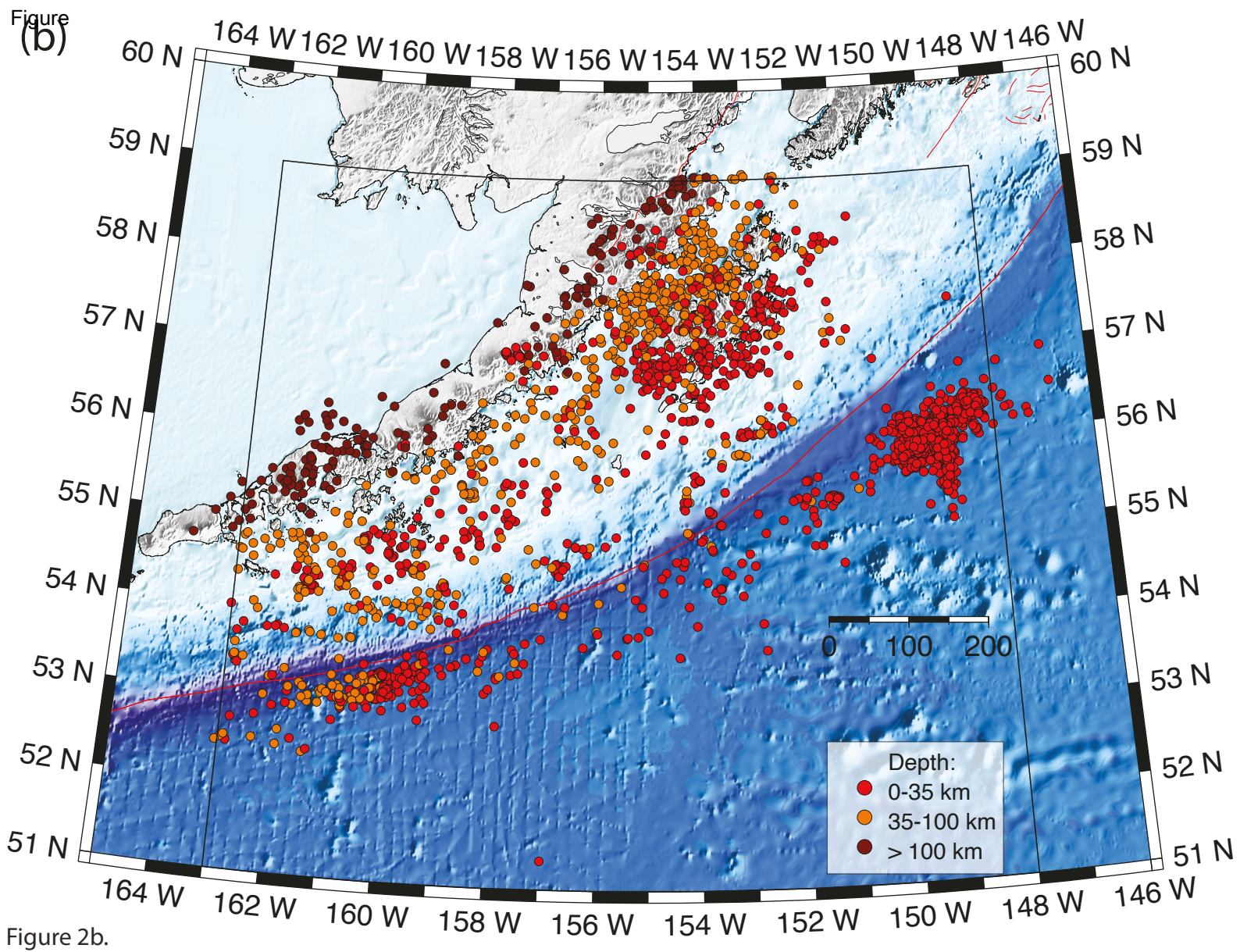
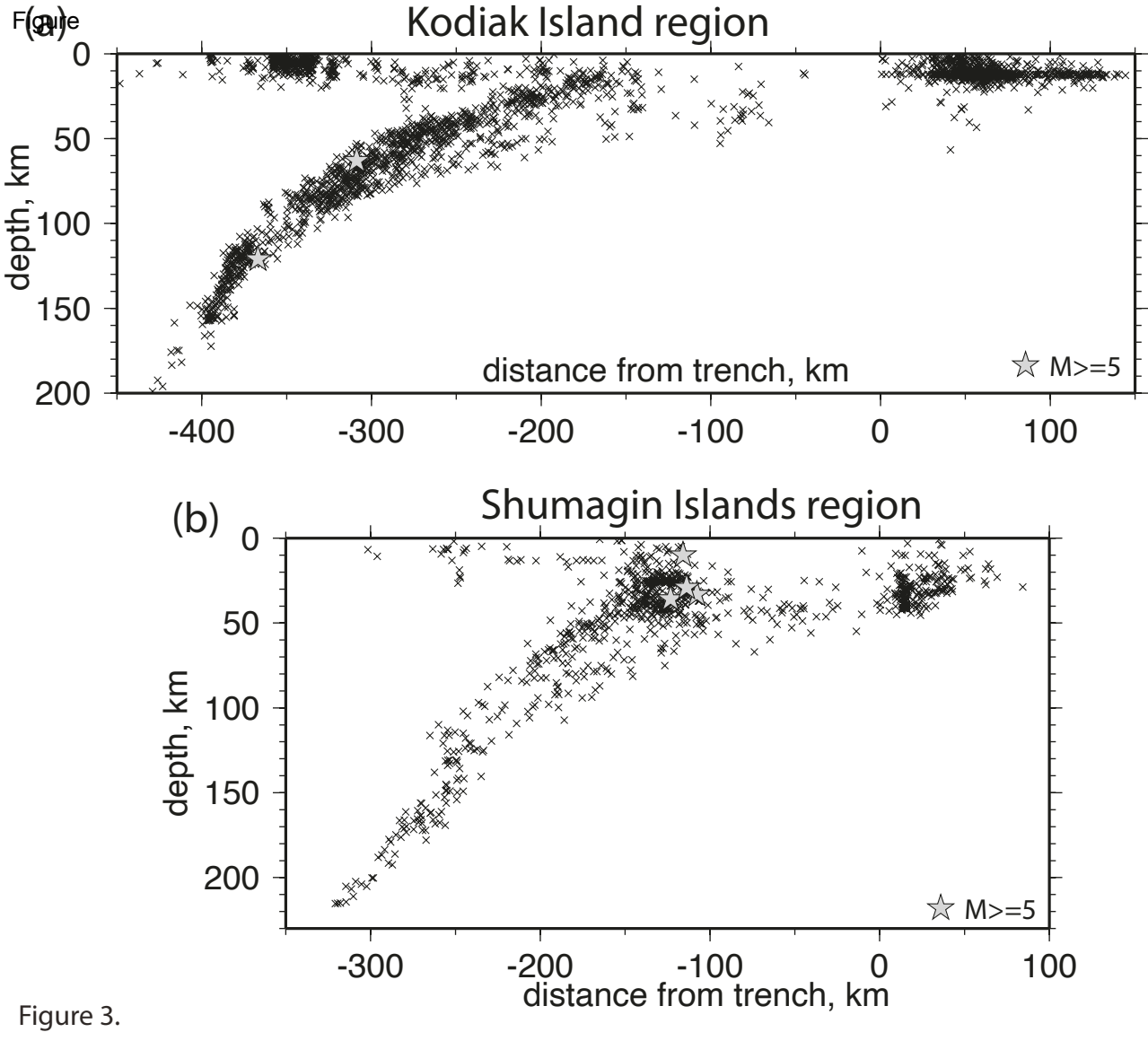


Figure 2a.





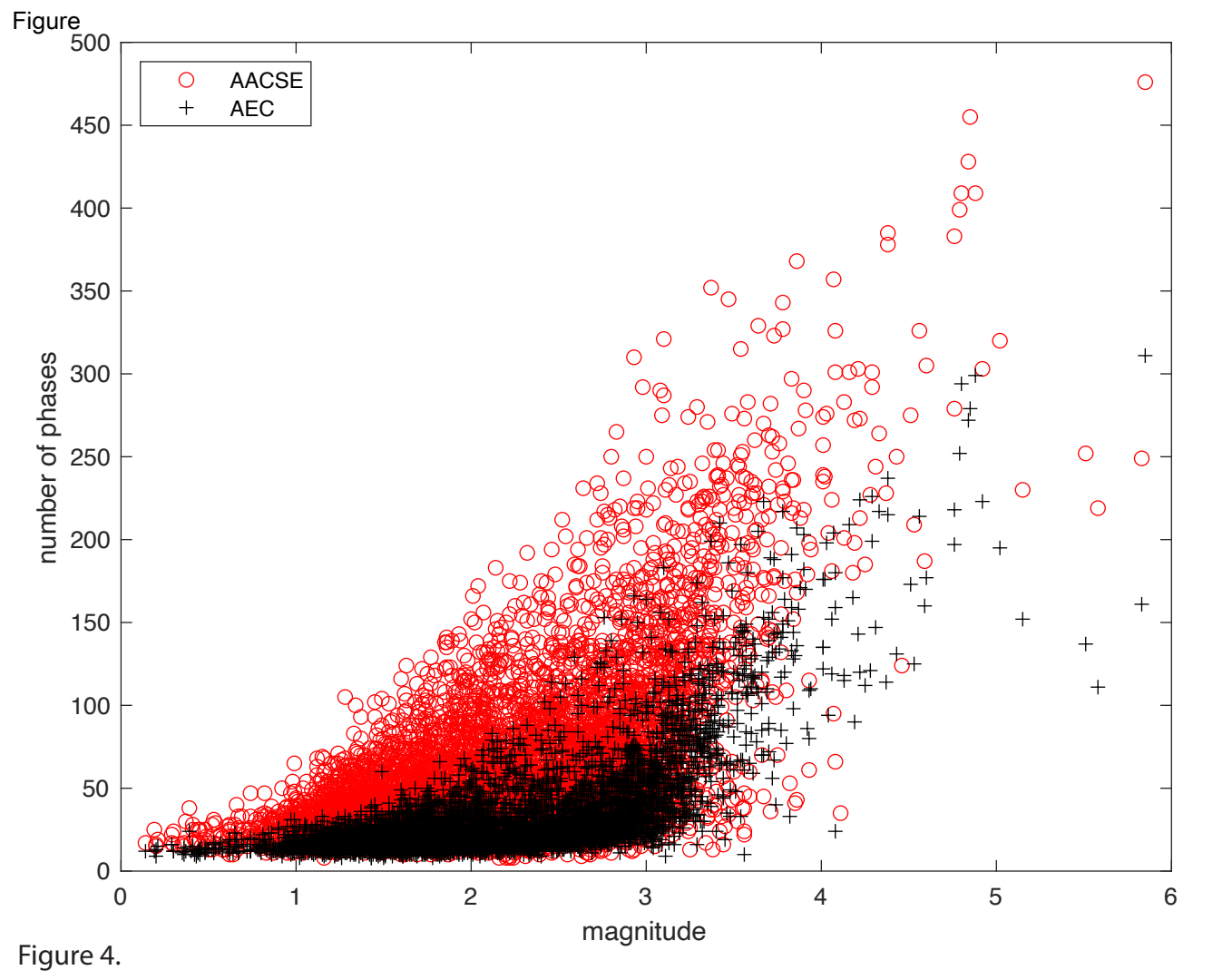
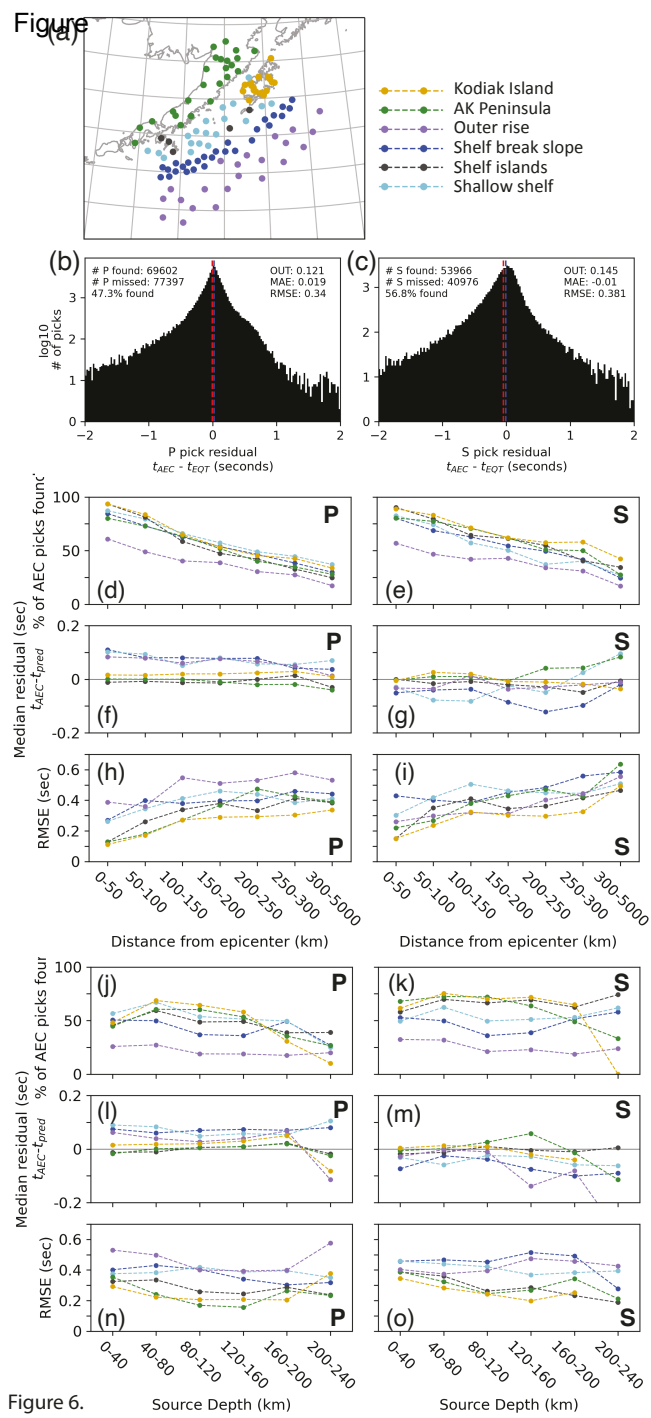


Figure 10<sup>4</sup> □ cumulative AK binned AK ☐ cumulative XO ■ binned XO 10<sup>3</sup> **Cumulative Number** 10<sup>1</sup> 00 10<sup>0</sup> 6 Magnitude

Figure 5.



## Supplemental Material for

## "Enhanced Regional Earthquake Catalog With Alaska Amphibious Community Seismic Experiment Data"

Natalia A. Ruppert<sup>1</sup>, Grace Barcheck<sup>2</sup>, and Geoffrey A. Abers<sup>2</sup>

1 – University of Alaska Fairbanks, Geophysical Institute, 2156 Koyukuk Drive, Fairbanks, Alaska 99775; <a href="mailto:naruppert@alaska.edu">naruppert@alaska.edu</a>; 907-474-7472 2 – Cornell University, Department of Earth and Atmospheric Sciences, 2160 Snee Hall, Ithaca, NY 14853

#### **Description**

This supplement contains additional tables and figures in support of the main article.

#### **Tables**

- **Table S1.** STA/LTA detection parameters.
- **Table S2.** Phase distance weighting used for computing hypocentral locations.
- **Table S3.** Velocity model *gulfak*.
- Table S4. Velocity model northak.
- **Table S5.** Velocity model *pavdut*.
- **Table S6**. Velocity model *scak*.
- **Table S7**. Monthly counts of analyzed events and picked seismic phases in AACSE earthquake catalog.
- **Table S8**. Parameters for 10 largest regional earthquakes recorded by the AACSE network.
- **Table S9**. Estimated magnitude of completeness for original AEC and enhanced AACSE earthquake catalogs.

#### **Figures**

- Figure S1. Travel time grids: (a) 0-50 km deep sources, and (b) 60-260 km deep sources.
- **Figure S2.** AACSE station magnitude residuals for land (top panel) and OBS (bottom panel) sites for AACSE catalog. Note systematic shift with distance for OBS sites. Residuals computed as the difference between network average of all observations for an event and individual station reading. Negative residuals indicate stations have higher than average amplitudes resulting in higher magnitudes.

- **Figure S3.** Travel-time residuals for regional and AACSE stations computed as average of predicted minus observed time based on all picks in AACSE catalog: (a) P-phase picks and (b) S-phase picks.
- **Figure S4**. Hypocentral location error histograms, binned in 2 km intervals. Mean error values for horizontal and vertical errors are 3.81 km and 2.46 km for AEC catalog and 1.83 km and 1.53 km for the AACSE catalog, respectively.
- **Figure S5**. Epicentral map of the M7.9 2018 Offshore Kodiak Earthquake aftershock region. Note systematic shift of the AACSE epicenters to the southeast.
- **Figure S6.** Histograms of pick time residuals binned by epicentral distance for all AACSE catalog picks found by EQTransformer with detection, P, and S thresholds of 0.3. Residuals are AEC AACSE catalog pick time minus EQT predicted pick time. Each row corresponds to an epicentral distance bin. The left column shows P pick residuals and the right column shows S pick residuals. Red and blue vertical lines show the mean and median residual, respectively. OUT is the fraction of residuals in the bin with an absolute value greater than 0.45 seconds. MAE is the mean absolute error in the bin, and RMSE is root mean squared error in the bin.
- **Figure S7**. Histograms of pick time residuals binned by earthquake depth for all AACSE catalog picks found by EQTransformer with detection, P, and S thresholds of 0.3. Residuals are AEC AACSE catalog pick time minus EQT predicted pick time. Each row corresponds to an earthquake depth bin. The left column shows P pick residuals and the right column shows S pick residuals. Red and blue vertical lines show the mean and median residual, respectively. OUT is the fraction of residuals in the bin with an absolute value greater than 0.45 seconds. MAE is the mean absolute error in the bin, and RMSE is root mean squared error in the bin.
- **Figure S8**. Histograms of pick time residuals binned by network region for all AACSE catalog picks found by EQTransformer with detection, P, and S thresholds of 0.3. Residuals are AEC AACSE catalog pick time minus EQT predicted pick time. Each row corresponds to a different region and instrument type in the AACSE network (corresponding to Figure 5). The left column shows P pick residuals and the right column shows S pick residuals. Red and blue vertical lines show the mean and median residual, respectively. OUT is the fraction of residuals in the bin with an absolute value greater than 0.45 seconds. MAE is the mean absolute error in the bin, and RMSE is root mean squared error in the bin.

**Table S1.** STA/LTA detection parameters.

Parameter	Land based stations	Ocean bottom stations	Pressure gauges	
Signal-to-noise detection "ON" threshold	3.5	4	3	
Signal-to-noise detection "OFF" threshold	2	2	2	
detection minimum "ON" time	2	2	1	
detection maximum "ON" time	10	10	5	
short term average time window	1	0.75	0.5	
short term average minimum time for average	1	1	1	
long term average time window	10	10	20	
long term average minimum time for average	5	5	5	
filter	BW 2.0 4 8.0 4	BW 4.0 4 7.0 4	BW 4.0 4 0.0 0	

 Table S2. Phase distance weighting used for computing hypocentral locations.

Distance, degrees	Weight
0.0	1.0
1.5	1.0
5.0	0.1
10.0	0.0

**Table S3.** Velocity model *gulfak*.

Depth to top (km)	P velocity (km/s)	S velocity (km/s)
0	5	2.9
7	6.8	3.8
12	8.1	4.5

 Table S5.
 Velocity model pavdut.

Depth to top (km)	P velocity (km/s)	S velocity (km/s)
0	3.05	1.71
3	3.44	1.93
4.79	5.56	3.12
6.65	6.06	3.4
13.18	6.72	3.78
25.63	7.61	4.28
41.51	7.9	4.44

 Table S4. Velocity model northak.

Depth to top (km)	P velocity (km/s)	S velocity (km/s)
0	5.9	3.3
24	7.4	4.2
40	7.9	4.4
76	8.29	4.7

**Table S6**. Velocity model *scak*.

Depth to top (km)	P velocity (km/s)	S velocity (km/s)
0	5.3	3.0
4	5.6	3.1
10	6.2	3.5
15	6.9	3.9
20	7.4	4.2
25	7.7	4.3
33	7.9	4.4
47	8.1	4.5
65	8.3	4.7

**Table S7**. Monthly counts of analyzed events and picked seismic phases in AACSE earthquake catalog.

	Events				Picks				
Year- Month	Old	New	Total	Percentage new	Old	New	Total	Percentage new	
2018-05	322	87	409	21	11,727	4,129	15,856	26	
2018-06	471	145	616	24	16,034	11,734	27,768	42	
2018-07	488	90	578	16	16,936	12,690	29,626	43	
2018-08	327	195	522	37	10,906	154,63	26,369	59	
2018-09	389	215	604	36	13,115	20,576	33,691	61	
2018-10	271	166	437	38	10,149	18,202	28,351	64	
2018-11	239	107	346	31	9,231	11,066	20,297	55	
2018-12	190	127	317	40	6,354	11,565	17,919	65	
2019-01	250	147	397	37	8,630	20,357	28,987	70	
2019-02	209	135	344	39	7,054	15,232	22,286	68	
2019-03	280	175	455	38	10,040	19,565	29,605	66	
2019-04	271	205	476	43	8,259	24,058	32,317	74	
2019-05	245	143	388	37	7,831	18,700	26,531	70	
2019-06	282	136	418	33	8,901	19,358	28,259	69	
2019-07	334	149	483	31	11,342	24,545	35,887	68	
2019-08	390	63	453	14	11,763	17,610	29,373	60	
Total	4,958	2,285	7,243	32	168,272	2648,50	4331,22	61	

**Table S8**. Parameters for the 10 largest regional earthquakes recorded by the AACSE network.\*

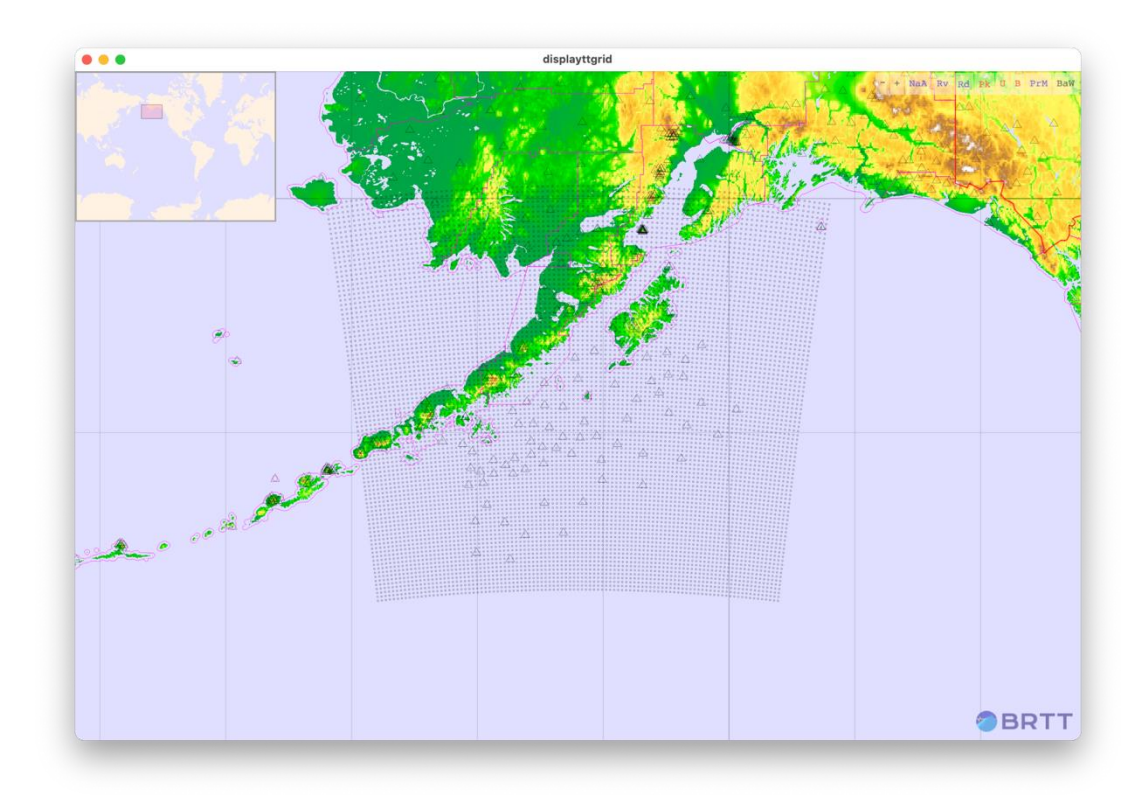
Date-Time (UTC)	Lat N	Lon W	Depth (km)	Mw w	stri ke	dip	slip	stri ke	dip	slip	Source type
7/18/18 19:06:04.27	54.3792	-160.7250	28.08	5.6	247	28	97	59	62	86	reverse
7/19/18 14:16:26.64	54.3439	-160.8068	33.09	5.8	246	22	97	58	68	87	reverse
7/21/18 07:58:40.88	54.3800	-160.7471	35.73	5.3	249	27	93	66	64	88	reverse
10/10/18 06:27:58.04	55.6233	-158.9113	60.56	5.0	224	70	-111	92	29	-46	normal
12/27/18 13:37:09.78	56.4035	-154.8155	53.57	4.95	163	74	-150	64	61	-18	oblique strike-slip
12/31/18 02:35:36.43	54.2840	-161.4468	35.83	6.0	240	31	96	52	59	86	reverse
1/02/19 06:48:43.72	58.3433	-153.1855	59.50	5.0	348	55	154	94	69	38	oblique strike-slip
1/22/19 04:43:19.43	58.3198	-155.2945	123.73	5.2	349	79	131	91	43	17	oblique strike-slip
2/15/19 22:54:19	53.4169	-162.8437	2.12	5.1	234	19	71	74	72	96	reverse
5/27/19 09:52:21.65	58.8509	-152.3565	66.50	5.8	327	72	163	62	74	19	strike-slip

<sup>\*</sup> Hypocentrer parameters are from AACSE earthquake catalog. Mww values and source parameters are from Comcat catalog.

**Table S9**. Estimated magnitude of completeness ( $M_{\text{C}}$ ) for original AEC and enhanced AACSE earthquake catalogs.

Region	AEC catalog Mc	AACSE catalog Mc
Entire region	2.7	2.5
Kodiak Island	1.6	1.4
Offshore Kodiak aftershocks	2.9	2.8
Outer rise	3.0	2.4
Shumagin Islands	2.1	2.1





(b)

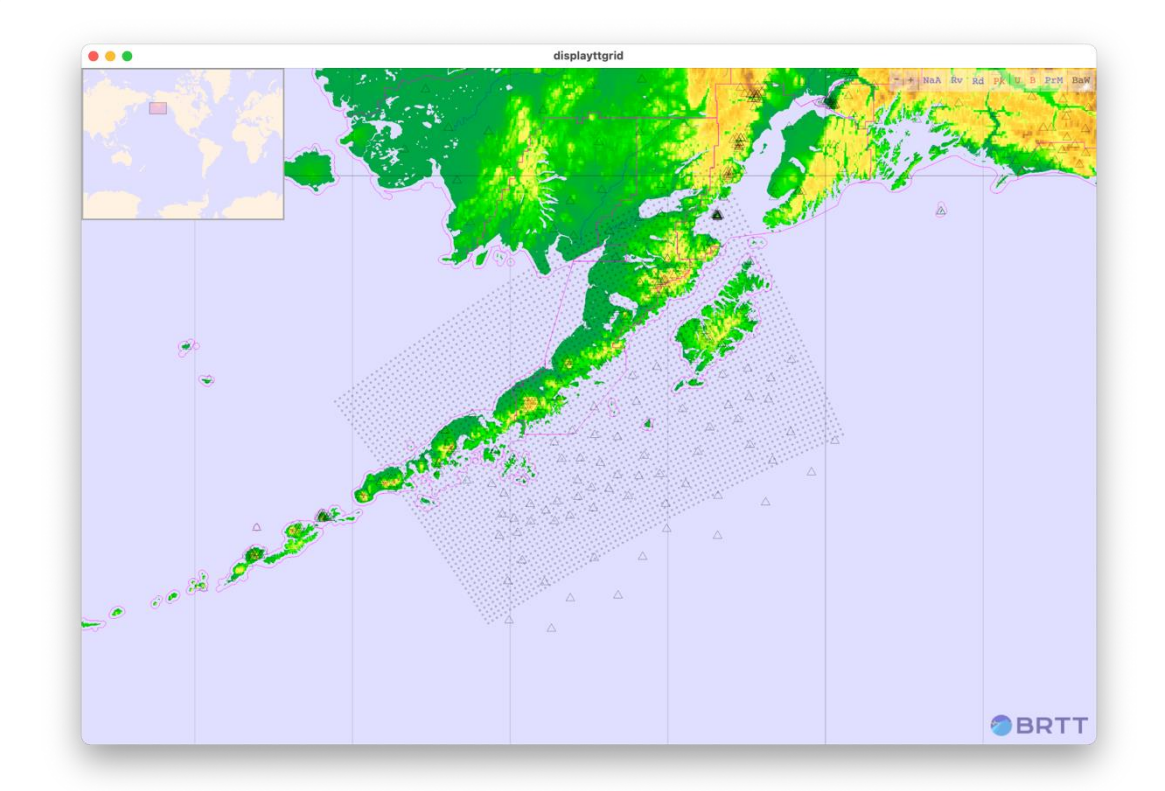
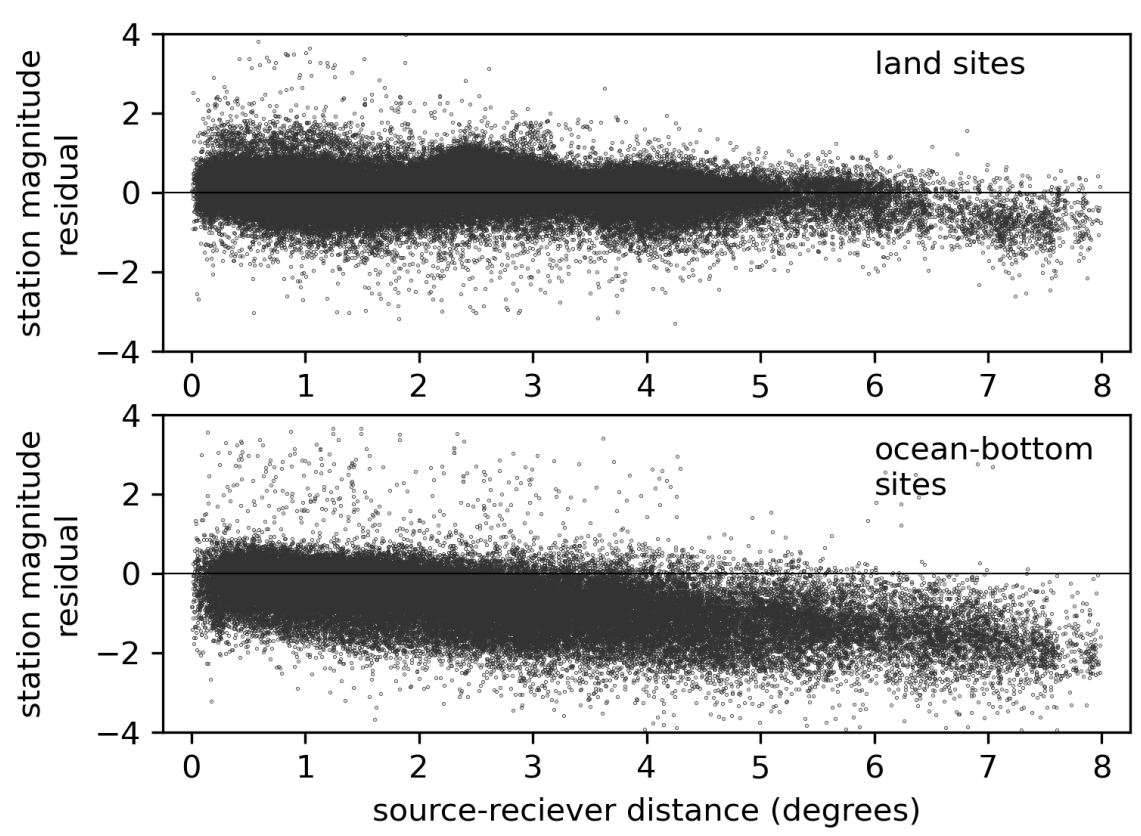


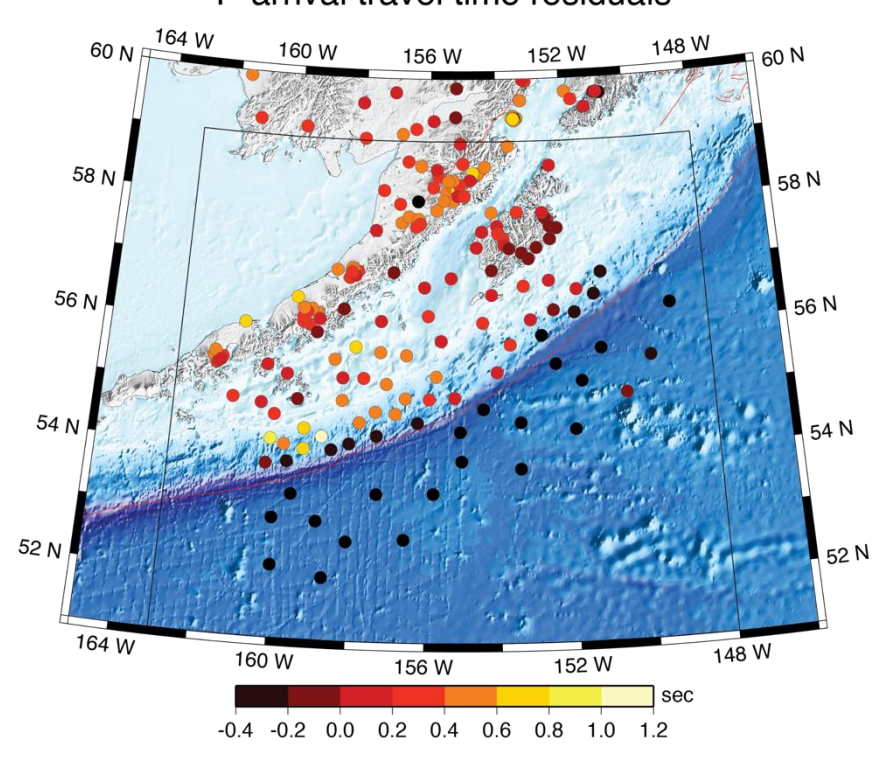
Figure S1. Travel time grids: (a) 0-50 km deep sources, and (b) 60-260 km deep sources.



**Figure S2.** AACSE station magnitude residuals for land (top panel) and OBS (bottom panel) sites for AACSE catalog. Note systematic shift with distance for OBS sites. Residuals computed as the difference between network average of all observations for an event and individual station reading. Negative residuals indicate stations have higher than average amplitudes resulting in higher magnitudes.



#### P-arrival travel time residuals



# (b) S-arrival travel time residuals

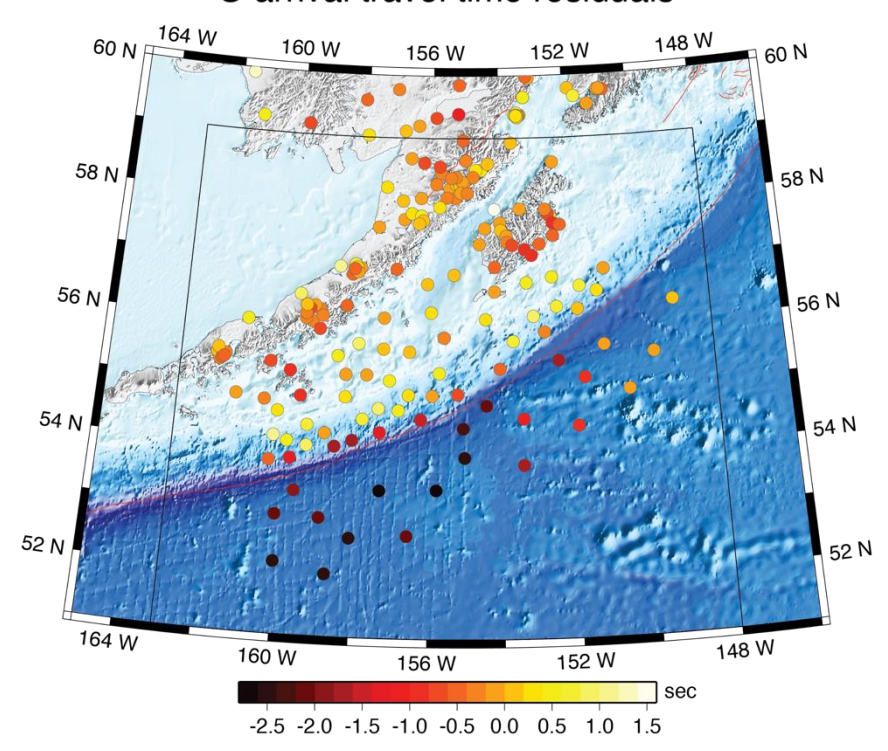


**Figure S3.** Travel-time residuals for regional and AACSE stations computed as average of predicted minus observed time based on all picks in AACSE catalog: (a) P-phase picks and (b) S-phase picks.

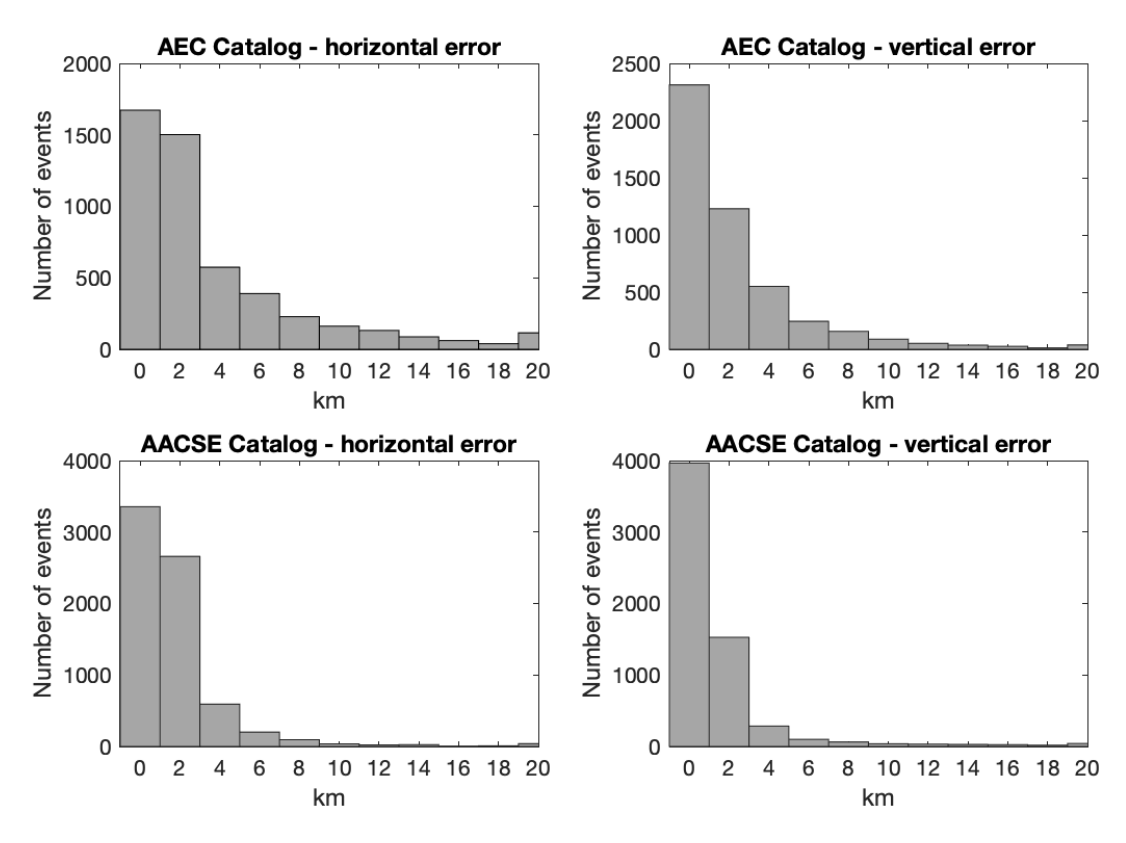


**Figure S4**. Hypocentral location error histograms, binned in 2 km intervals. Mean error values for horizontal and vertical errors are 3.81 km and 2.46 km for AEC catalog and 1.83 km and 1.53 km for the AACSE catalog, respectively.

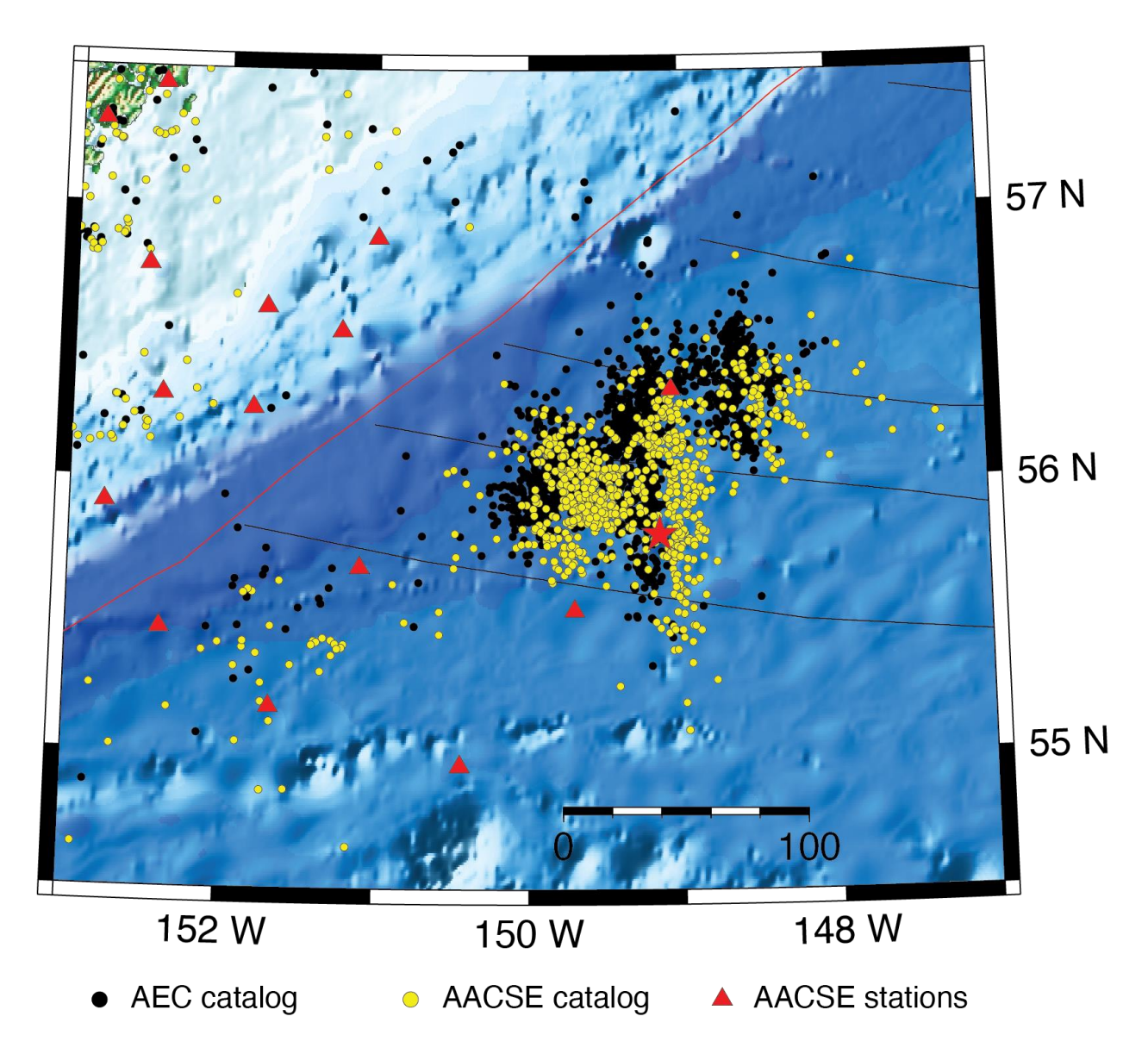


**Figure S5**. Epicentral map of the M7.9 2018 Offshore Kodiak Earthquake aftershock region. Note systematic shift of the AACSE epicenters to the southeast.

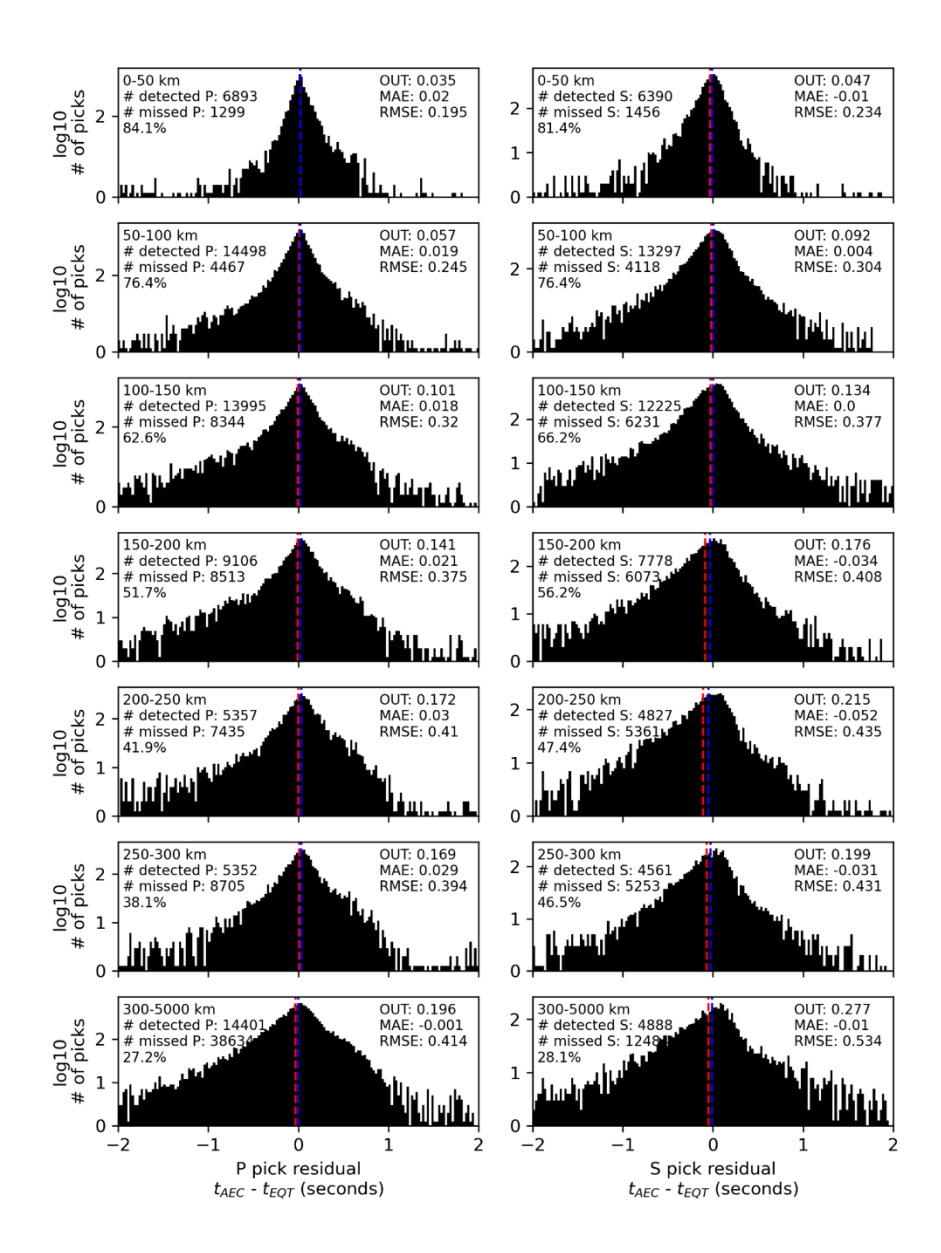


**Figure S6.** Histograms of pick time residuals binned by epicentral distance for all AACSE catalog picks found by EQTransformer with detection, P, and S thresholds of 0.3. Residuals are AEC AACSE catalog pick time minus EQT predicted pick time. Each row corresponds to an epicentral distance bin. The left column shows P pick residuals and the right column shows S pick residuals. Red and blue vertical lines show the mean and median residual, respectively. OUT is the fraction of residuals in the bin with an absolute value greater than 0.45 seconds. MAE is the mean absolute error in the bin, and RMSE is root mean squared error in the bin.

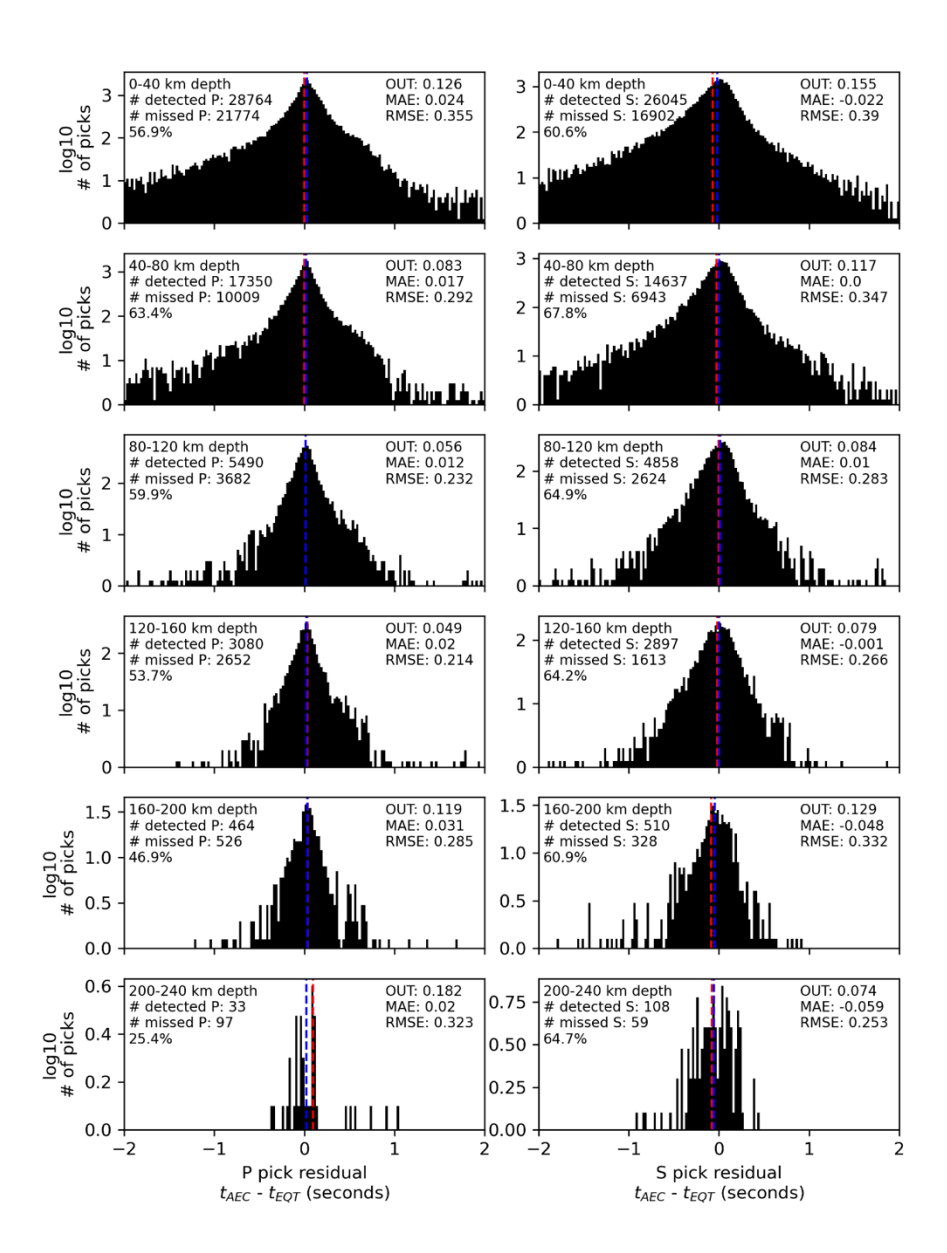


**Figure S7**. Histograms of pick time residuals binned by earthquake depth for all AACSE catalog picks found by EQTransformer with detection, P, and S thresholds of 0.3. Residuals are AEC AACSE catalog pick time minus EQT predicted pick time. Each row corresponds to an earthquake depth bin. The left column shows P pick residuals and the right column shows S pick residuals. Red and blue vertical lines show the mean and median residual, respectively. OUT is the fraction of residuals in the bin with an absolute value greater than 0.45 seconds. MAE is the mean absolute error in the bin, and RMSE is root mean squared error in the bin.

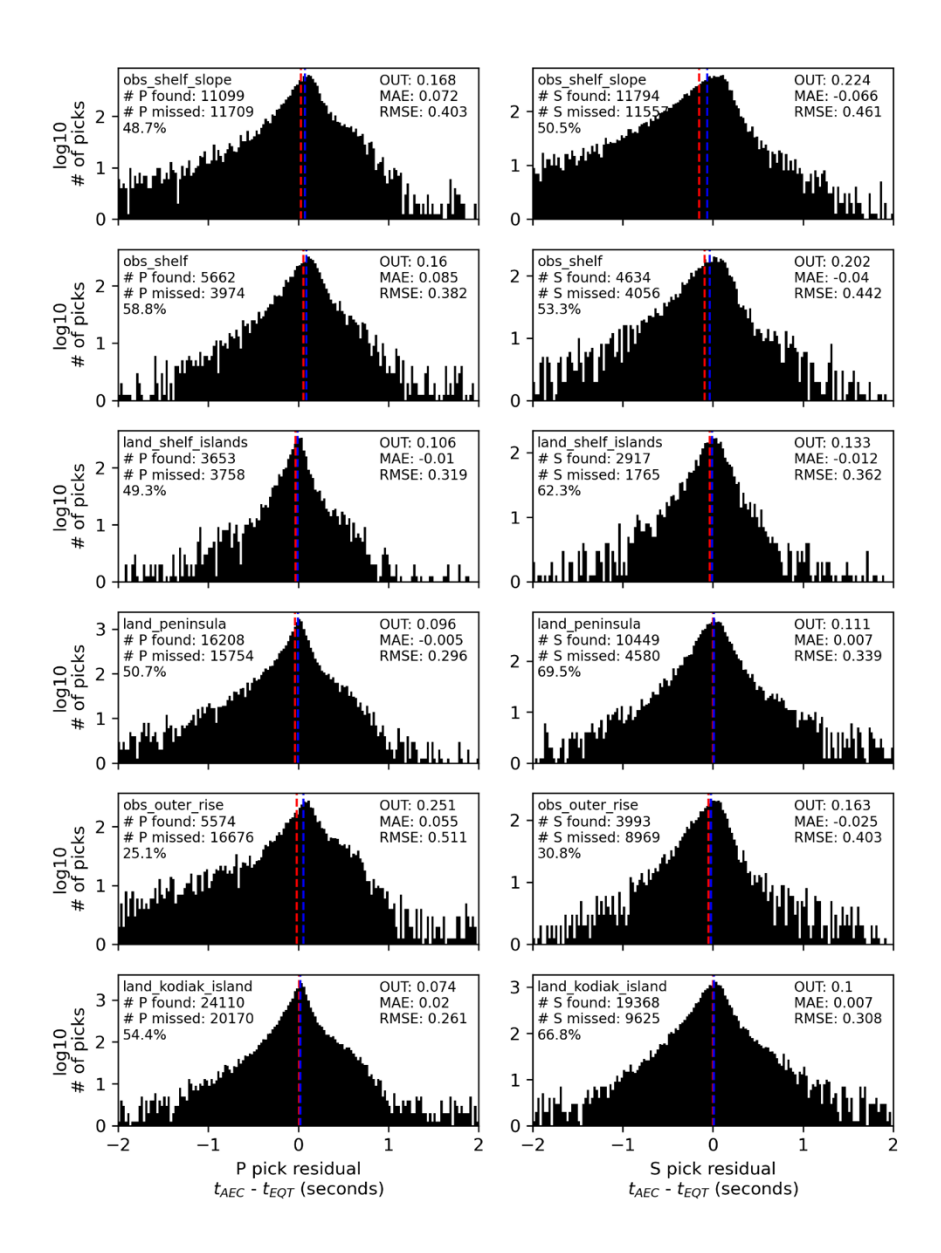


**Figure S8**. Histograms of pick time residuals binned by network region for all AACSE catalog picks found by EQTransformer with detection, P, and S thresholds of 0.3. Residuals are AEC AACSE catalog pick time minus EQT predicted pick time. Each row corresponds to a different region and instrument type in the AACSE network (corresponding to Figure 5). The left column shows P pick residuals and the right column shows S pick residuals. Red and blue vertical lines show the mean and median residual, respectively. OUT is the fraction of residuals in the bin with an absolute value greater than 0.45 seconds. MAE is the mean absolute error in the bin, and RMSE is root mean squared error in the bin.